On a spectral method for forward gravity field modelling

Root, B. C.; Novák, P.; Dirkx, D.; Kaban, M.; van der Wal, W.; Vermeersen, L. L A

DOI
10.1016/j.jog.2016.02.008

Publication date
2016

Document Version
Accepted author manuscript

Published in
Journal of Geodynamics

On a spectral method for forward gravity field modelling

B.C. Root[a], P. Novák[b], D. Dirkx[a,d], M. Kaban[c,f], W.van der Wal[a], L.L.A. Vermeersen[a,e]

[a] *Delft University of Technology, Kluyverweg 1, 2629 HS Delft, The Netherlands*
[b] *University of West Bohemia, Univerzitni 8, 306 14 Pilsen, Czech Republic*
[c] *Helmholtz Center Potsdam, GFZ German Research Center for Geosciences, Potsdam, Germany*
[d] *Joint Institute for VLBI ERIC, PO Box 2, 7990 AA Dwingeloo, The Netherlands*
[e] *NIOZ, Korringweg 7,4401 NT Yerseke, the Netherlands*
[f] *Schmidt Institute of Physics of the Earth, RAS, Moscow, Russia*

Abstract

This article reviews a spectral forward gravity field modelling method that was initially designed for topographic/isostatic mass reduction of gravity data. The method transforms 3D spherical density models into gravitational potential fields using a spherical harmonic representation. The binomial series approximation in the approach, which is crucial for its computational efficiency, is examined and an error analysis is performed. It is shown that, this method cannot be used for density layers in crustal and upper mantle regions, because it results in large errors in the modelled potential field. Here, a correction is proposed to mitigate this erroneous behaviour. The improved method is benchmarked with a tesseroid gravity field modelling method and is shown to be accurate within ± 4 mGal for a layer representing the Moho density interface, which is below other errors in gravity field studies. After the proposed adjustment the method can be used for the global gravity modelling of the complete Earth's density structure.

Keywords: forward gravitational field modelling, spherical harmonic representation, global density models

1. Introduction

Interpreting gravitational data in terms of internal mass density distributions requires gravitational reduction that can be computed by forward modelling

techniques. The gravitational field of any 3-D object can be computed by integrating the gravitational effects of its mass density distribution. One technique for evaluating this integral is based on spherical harmonic expansion of the Newtonian kernel. This technique was applied to forward modelling of the topographic potential and its gradients (*Lachapelle*, 1976; *Rapp*, 1982; *Rummel et al.*, 1988; *Pavlis and Rapp*, 1990) and modified for computing gravitational gradients generated by topography and atmosphere at satellite altitudes (*Novák and Grafarend*, 2006). The advantage of this technique is that it takes into account the curvature of the Earth.

There are two approaches to solve the spherical harmonic-based volume integral (*Pavlis and Rapp*, 1990): the rigorous formulation and the binomial series expansion method. The rigorous spectral method (RSM) introduced by *Lachapelle* (1976) is computational expensive (*Pavlis and Rapp*, 1990). The second approach, by *Rummel et al.* (1988), uses a binomial series expansion to approximate the volume. We call it the Fast Spectral Method (FSM) in this study, because it is computationally more efficient than the rigorous spectral method. The number of computationally expensive global spherical harmonic analyses (GSHA) (*Sneeuw*, 1994) is drastically reduced by introducing the binomial series approximation. The FSM approach provides a means to use higher resolution density models than the RSM.

The FSM forward modelling is used in several previous studies (*Rummel et al.*, 1988; *Novák and Grafarend*, 2006; *Martinec*, 1991; *Root et al.*, 2015). Despite its computational speed, the FSM has limitations that should be known to users. The FSM forward modelling is used to compute the potential field of a topographic/isostatic mass layer in most studies, but for density layers in the lower crust and upper mantle the FSM gives erroneous results as will be shown in Section 4. This erroneous signal results in incorrect mantle density heterogeneities, when the FSM is used in a gravity inversion study. The improvement which is introduced here extends the applicability of the FSM to the general case of forward gravitational modelling of mass density distributions for an entire planet.

Section 2 provides a review of the analytical representation of the FSM. This is followed by a characterisation of the error introduced by the binomial series approximation. In Section 4, a mitigation strategy is introduced. Finally, a benchmark of the FSM with tesseroid software is shown in Section 5.

2. Review of the fast spectral forward modelling method

The analytical representation of the RSM and FSM starts similarly (*Pavlis and Rapp*, 1990). In the following, we derive a formula for the gravitational potential which is the conventional representation of a (conservative and irrotational) gravitational field. From Newton's law of universal gravitation and the superposition principle, the gravitational potential V outside the body Σ at location, P, can be computed (e.g.*Rummel et al.* (1988)):

$$V(P) = G \iiint_{\Sigma} \frac{\rho(Q)}{\ell(P,Q)} \, \mathrm{d}\Sigma(Q) \; . \tag{1}$$

where G is the universal gravitational constant, ρ is the mass density distribution within the body Σ and $\ell(P,Q)$ is the Euclidian distance between the computation point $P(r,\Omega)$ and the infinitesimal volume element $\mathrm{d}\Sigma(Q)$ at location $Q(r',\Omega')$. Eq. (1) can be rewritten by using (geocentric) spherical coordinates:

$$\mathrm{d}\Sigma = r^2 \mathrm{d}r\mathrm{d}\Omega. \tag{2}$$

Here, r is the radial coordinate and $\mathrm{d}\Omega = \sin(\theta)\mathrm{d}\theta\mathrm{d}\lambda$ is a surface element at a unit sphere, where ϕ and λ stand for a pair of geocentric angular coordinates and represents a geocentric direction. Eq. (1) then becomes

$$V(r,\Omega) = G \int_{\Xi} \int_{r'=r_{lower}(\Omega')}^{r_{upper}(\Omega')} \rho(r',\Omega') \; \mathcal{L}^{-1}(r,\Omega,r',\Omega') \; r'^2 \; \mathrm{d}r' \; \mathrm{d}\Omega' \; . \tag{3}$$

The kernel function $\mathcal{L}^{-1}(r,\Omega,r',\Omega') = \frac{1}{\ell(P,Q)}$ and the radial coordinate is given by r'. The radial limits of this integral represent the upper and lower boundaries of the mass density layer. The spherical harmonic representation for the inverse distance kernel is (*Heiskanen and Moritz*, 1984, p. 33):

$$\mathcal{L}^{-1}(r,\Omega,r',\Omega') = \frac{1}{r} \sum_{n,m}^{\infty} \left(\frac{r'}{r}\right)^n \frac{1}{2n+1} \; Y_{nm}(\Omega) \; Y^*_{nm}(\Omega') \; . \tag{4}$$

In this equation the abbreviated notation $\sum_{n,m}^{\infty} = \sum_{n=0}^{\infty} \sum_{m=-n}^{n}$ is used. Eq. (4) can be substituted in Eq. (3):

$$V(r,\Omega) = G\sum_{n,m}^{\infty}\left(\frac{1}{r}\right)^{n+1}\frac{1}{2n+1}\,Y_{nm}(\Omega)\int\limits_{\Xi}\rho(\Omega')\,Y_{nm}^{*}(\Omega')\,\mathrm{d}\Omega'\int\limits_{r_{lower}(\Omega')}^{r_{upper}(\Omega')} r'^{n+2}\mathrm{d}r'\,. \tag{5}$$

where it is assumed that the density distribution within the layer does not depend on the radial position. Appendix A discusses an approach for a radially varying density distribution in the mass layer. For both cases, the radial integral in Eq. (5) must be evaluated. The radial limits of this integral can be defined as follows:

$$r_{upper}(\Omega') = R + U(\Omega')\,, \tag{6a}$$

$$r_{lower}(\Omega') = R + L(\Omega')\,. \tag{6b}$$

$U(\Omega')$ and $L(\Omega')$ are upper and lower deviations from the circumscribing sphere (R) of the volumetric mass layer that is forward modelled (see Figure 1). This means that $R \geq R+U \geq R+L$, or in other words $0 \geq U \geq L$. Integrating the radial integral of Eq. (5) then yields

$$\int\limits_{r_{lower}(\Omega')}^{r_{upper}(\Omega')} r'^{n+2}\,\mathrm{d}r' = \frac{1}{n+3}\left\{\underbrace{[R+U(\Omega')]^{n+3}}_{1^{st}\text{ part}} - \underbrace{[R+L(\Omega')]^{n+3}}_{2^{nd}\text{ part}}\right\}. \tag{7}$$

From this point the RSM and the FSM differ. In the RSM a global spherical harmonic analysis (GSHA) is performed on Eq. (7) to determine the spherical harmonic coefficients of the potential field (*Lachapelle*, 1976). However, this is computationally expensive, because for every degree (n) an individual GSHA must be performed. Especially, when the spherical harmonic degree is large the time to compute the potential field is unpractical. The FSM was developed to tackle this problem.

In the FSM, the first and second part in Eq. (7) can be evaluated by a binomial series expansion (*Abramowitz and Stegun*, 1972). Writing $n+3=\nu$ and replacing U and L by their normalised values $\tilde{U}=\frac{U}{R}$ and $\tilde{L}=\frac{L}{R}$, we get

$$(R+U)^{\nu} - (R+L)^{\nu} = R^{\nu}\sum_{k=0}^{\nu}\binom{\nu}{k}\left[\,\tilde{U}^{k} - \tilde{L}^{k}\right]. \tag{8}$$

The series summation contains a finite number of terms, as ν is a positive integer (*Abramowitz and Stegun*, 1972). To reduce the computational load,

in practical applications (*Rummel et al.*, 1988) this series is truncated at a value α, where $\alpha < \nu$, resulting in

$$(R+U)^\nu - (R+L)^\nu = R^\nu \sum_{k=0}^{\alpha} \binom{\nu}{k} \left[\; \tilde{U}^k - \tilde{L}^k \; \right] + \epsilon_\alpha \; . \tag{9}$$

Here, ϵ_α is the error made by the truncation of the binomial series. An error analysis of this assumption follows in Section 3.1, but for now we will choose $\alpha = 3$ (*Rummel et al.*, 1988). By neglecting the higher-order terms, the radial integral from Eq. (7) becomes

$$\int_{r_{lower}(\Omega')}^{r_{upper}(\Omega')} r'^{n+2} \, \mathrm{d}r' \approx R^{n+3} \left[\; \frac{U(\Omega') \; - \; L(\Omega')}{R} \; + \; (n+2) \frac{U^2(\Omega') \; - \; L^2(\Omega')}{2R^2} \right.$$
$$\left. + \, (n+2)(n+1) \; \frac{U^3(\Omega') \; - \; L^3(\Omega')}{6R^3} \; \right] . \tag{10}$$

Following *Novák and Grafarend* (2006), we will use a short-hand notation, $F(\Omega')$, to denote everything between the square brackets of Eq. (10):

$$\int_{r_{lower}(\Omega')}^{r_{upper}(\Omega')} r'^{n+2} \, \mathrm{d}r' \approx R^{n+3} F(\Omega') \; . \tag{11}$$

Substituting Eq. (11) in Eq. (5) gives:

$$V(r,\Omega) = GR^2 \sum_{n,m}^{\infty} \left(\frac{R}{r} \right)^{n+1} \frac{1}{2n+1} \; Y_{nm}(\Omega) \int_{\Xi} \rho(\Omega') \; F(\Omega') \; Y^*_{nm}(\Omega') \; \mathrm{d}\Omega' \; . \tag{12}$$

Novák and Grafarend (2006) continue by performing GSHA of the density distribution function $\rho(\Omega')$ and the function $F(\Omega')$ separately. The spherical harmonic coefficients retrieved from the two separate GSHA procedures are combined in the spherical harmonics domain using complex Glebsch-Gordan series. However, the same result can be obtained by multiplying the mass density distribution $\rho(\Omega')$ with the function $F(\Omega')$ in the spatial domain and by subsequent GSHA of the combined function, i.e.,

$$\rho(\Omega') \; F(\Omega') \; \stackrel{GSHA}{=} \; \sum_{n,m}^{\infty} C_{nm} \; Y_{nm}(\Omega') \; . \tag{13}$$

Coefficients C_{nm} are derived from the density and geometry of the modelled layer. This approach requires one less GSHA which is favourable, because a GSHA is computationally expensive. Substituting Eq. (13) into Eq. (12) and reordering the integral and summation yields:

$$V(r,\Omega) = GR^2 \sum_{n,m}^{\infty} \left(\frac{R}{r}\right)^{n+1} \frac{1}{2n+1}\, Y_{nm}(\Omega) \times \sum_{n',m'}^{\infty} C_{n'm'} \int_{\Xi} Y_{n'm'}(\Omega')\, Y^*_{nm}(\Omega') \mathrm{d}\Omega' \,. \tag{14}$$

Using the orthogonality of fully-normalized spherical harmonic functions (*Heiskanen and Moritz*, 1984, p. 29) results in

$$V(r,\Omega) = GR^2 \sum_{n,m}^{\infty} \left(\frac{R}{r}\right)^{n+1} \frac{4\pi}{2n+1}\, C_{nm}\, Y_{nm}(\Omega) \,. \tag{15}$$

To compare the gravitational potential of the layer with global gravitational models referenced to a particular gravitational constant GM, the potential should be scaled accordingly using the following relation:

$$(GM)^{model} = \frac{4}{3}\, \pi\, \rho_E\, G\, R^3 \,. \tag{16}$$

in which, ρ_E is the average mass density of the reference Earth computed with GM and R from the global gravitational model. Substituting Eq. (16) into (15), yields:

$$V(r,\Omega) = \frac{GM}{R} \sum_{n,m}^{\infty} \left(\frac{R}{r}\right)^{n+1} V_{nm}\, Y_{nm}(\Omega) \tag{17}$$

with

$$V_{nm} = \frac{3}{2n+1}\, \frac{1}{\rho_E}\, C_{nm} \,. \tag{18}$$

The coefficients, V_{nm}, are referred to as the Stokes coefficients. The constructed gravitational potential is derived for a particular mass density layer in an Earth model. A more complex model can be built by adding the potential of several layers.

3. Error characterisation of the fast spectral method

In the derivations of the FSM, higher-order terms of the binomial series expansion were neglected to arrive to Eq. (10). Previous studies suggested

that an expansion up to the third-order binomial term is enough to accurately model the gravitational potential of a topographic layer (*Rummel et al.*, 1988; *Vaníček et al.*, 1995). However, with the increasing accuracy of gravitational, digital elevation (DEM), and crustal models, the question arises if this finding is still valid. This section describes the effect of the binomial order truncation in Eq. (9) on the accuracy of the forward modelled gravitational potential. Moreover, we examine if this assumption is still valid for deeper layers.

It will be shown that the truncation of the binomial series introduces errors for layers that deviate substantially from the radius of the reference sphere, R, which cannot be reduced by truncating at a higher order. This is the case for crustal and upper mantle mass layers. To extend the capabilities of the FSM to deeper layers, an improved forward model is presented. First the error due to the truncation of the binomial series is discussed.

3.1. Characterisation of the truncation error

From Eq. (9) the error ϵ_α follows as:

$$\epsilon_\alpha = R^\nu \sum_{k=\alpha+1}^{\nu} \binom{\nu}{k} \left[\tilde{U}^k - \tilde{L}^k \right] = R^\nu \sum_{k=\alpha+1}^{\nu} \epsilon^{(k)}, \tag{19}$$

where $\epsilon^{(k)}$ is a shorthand notation for the k^{th} term in the summation. Our goal here is to find the smallest order at which the series can be truncated without introducing a substantial error in the results. To do so, we will derive a criterion that allows us to quantify the relative contribution of the leading order term $\epsilon^k (= \epsilon^{\alpha+1})$ in Eq. (26), compared to the entire error ϵ_α. In doing so, we quantify the reduction in the error that results from increasing α by 1.

To show how $\epsilon^{(k)}$ changes with increasing k, and thereby how ϵ_α changes with increasing α, we construct a variable $C^{(k)}$

$$C^{(k)} = \left| \frac{\epsilon^{(k+1)}}{\epsilon^{(k)}} \right| = \left| \frac{\nu - k}{k+1} \frac{\left[\tilde{U}^{k+1} - \tilde{L}^{k+1} \right]}{\left[\tilde{U}^k - \tilde{L}^k \right]} \right| . \tag{20}$$

For $k = \alpha$, this variable is the relative change in the magnitude of the first term in Eq. (19), $\epsilon^{(\alpha+1)}$, when α is increased by one, so when Eq. (9) is truncated one order higher. Thus, it is a measure of the change in the first error term when adding an extra term to the binomial series. Since $\frac{\nu-k}{k+1}$ is

continuously decreasing with k, and it can be numerically checked that this is also the case for $\left|\frac{\tilde{U}^{k+1}-\tilde{L}^{k+1}}{\tilde{U}^{k}-\tilde{L}^{k}}\right|$ for any practical values of $\tilde{U}$ and $\tilde{L}$, it follows that

$$C^{(k+1)} < C^{(k)}. \tag{21}$$

However, in theory there could be cases where $C^{(k)} \geq 1$ and $C^{(k)} \approx C^{(k+1)}$. The error made when truncating Eq. (9) will not decrease substantially when adding a single additional term (*i.e.* when increasing α by 1). In fact, when $C^{(k)} > 1$, $\epsilon^{(k)}$ increases with k and increasing α by 1 will not even remove the largest error term.

Therefore, a stringent requirement is needed on $C^{(k)}$ to study the region where all remaining error terms are relatively small compared to the current leading order term, and increasing α by 1 will cause a substantial reduction of the total error. Such a requirement can be derived from Eq. (21) and from the fact that:

$$\sum_{k=2}^{l_{max}} \frac{1}{2^k} < \frac{1}{2}, \tag{22}$$

for any finite l_{max}. The following criterion has to be met:

$$C^{(k)} \leq \frac{1}{2}. \tag{23}$$

This ensures that adding a single term to the binomial expansion will decrease the total error by *at least* a factor of 2 and that all remaining error terms will not be dominant compared to the current leading order error term:

$$\epsilon^{(k)} > \sum_{l=k+1}^{\nu} \epsilon^{(l)}. \tag{24}$$

Although this criterion (Eq. (23)) provides no guarantee that the total error is acceptable, it does follow that if Eq. (23) is not met, the error properties of higher order terms will be relatively influential and as a result α will likely need to be increased considerably to attain an acceptable error level. The criterion (23) will be called the convergence criterion.

Now that we have established a convergence criterion, we can compute the appropriate truncation limit for a potential field with a certain spherical

harmonic resolution. For a given geometry (defined by $\tilde{U}$ and $\tilde{L}$) and truncation level α, using the convergence criterion in Eq. (23) yields the following condition for ν

$$\nu < \left| \frac{1}{2} \frac{\tilde{U}^{\alpha} - \tilde{L}^{\alpha}}{\tilde{U}^{\alpha+1} - \tilde{L}^{\alpha+1}} \left(\alpha + 1\right) + \alpha \right| , \tag{25}$$

where we have set $k = \alpha$ in Eq. (23). We reiterate that $\nu = n+3$ and therefore ν indicates the maximum degree of the spherical harmonic expansion. From this relation it is clear that for thicker layers, for which $|\tilde{U} - \tilde{L}|$ is larger, ν has to be smaller than the limit in order for (23) to hold, as the influence of higher order terms in Eq. (9) increases. Similarly, for deeper layers, in which the magnitude of both $\tilde{U}$ and $\tilde{L}$ are increased by the same amount, the influence of the higher order terms is also stronger.

When we use a simplified geometry of an arbitrary mass layer in which we set the upper limit U equal to the circumscribing sphere, so that $\tilde{U}$ becomes 0, we obtain the following:

$$\nu < \left| \frac{\alpha + 1}{2\tilde{L}} + \alpha \right| \approx \frac{\alpha + 1}{2\tilde{L}}, \tag{26}$$

where the approximation follows from the fact that typically $\tilde{L} \ll 1$. The above equation will still approximately hold true in cases where $|L| \gg |U|$, in which the upper limit of the entire boundary is close to, but not exactly on, the circumscribing sphere (relative to the thickness of the layer). The convergence criterion of equations (25) and (26) shows the following relation $\epsilon^{(k)} > \sum_{l=k+1}^{\nu} \epsilon^{(l)}$.

To illustrate the behaviour of $C^{(k)}$ with varying geometry and truncation level, we show its behaviour as a function of k and U in Figure 2, for a number of spherical harmonic degrees and layer thicknesses. Note that larger absolute values of U mean that the layer starts at a distance further away from the circumscribing sphere with radius R. It can be seen from Figure 2 that the value of $C^{(k)}$ is lower for a given value of k when (i) the layer is thinner, (ii) the layer starts closer to the reference sphere, and (iii) the spherical harmonic degree is smaller. Furthermore, Figure 2 shows that as k increases, the rate at which $C^{(k)}$ decreases levels off. In certain cases, this property can be advantageous for the practical application of Eq. (19), as it means that the majority of the error can be located in the low values of k. However, this no longer holds when $C^{(k)} > 1$, for which $\epsilon^{(k)}$ is increasing with k. In Figure 2, the $\alpha = 3$ truncation level that is typically used (*Rummel*

et al., 1988) is shown by a dashed vertical line. The intersection of this line with the $C^{(k)} = 0.5$ contour represents the point above which the binomial series expansion fails to comply with Eq. (23). From this level on, it cannot be assumed that the remaining error due to the truncation of the binomial series is small.

Figure 3 plots the spherical harmonic degree ν with respect to the value of the upper boundary U of the layer for the binomial order truncation, $\alpha = 3$. The value for U is an approximate representation for the deviation from the reference radius R. The characteristic degree that fulfils the convergence criterion quickly drops to low values when the depth of the layer increases. For layers with a depth of 100 km, spherical harmonic coefficients from around degree 80 and above contain large errors due to the truncation. At a depth of 200 km coefficients from degree and order 50 are affected, at 300 km coefficients from degree and order 30 are affected and at 400 km coefficients from degree and order 25 are affected.

For this study we use the spherical approximation, but for high-accuracy applications the ellipsoidal approximation is used. *Claessens and Hirt* (2013) use the same approach concerning the binomial series approximation, which is characteristic of the FSM, and truncate it after a few order of the binomial series. This is correct for topographic reduction, but we would expect similar errors occur in the ellipsoidal approximation when deeper density layers are forward modelled. The magnitude of these effects needs to be further investigated, but is outside the scope of this study.

3.2. Numerical error characterisation for topographic masses

If the convergence criterion is fulfilled the remaining error of the FSM for an arbitrary mass layer can be determined numerically, because the extra signal from an added binomial term is larger than the remaining error. Thus, it is an estimate of the maximum error at a certain binomial order truncation.

We use a topographic mass layer to numerically estimate the error. The topographic mass reduction is derived from the global digital elevation model GTOPO30 reduced to a 0.1 x 0.1 arc-deg equiangular grid. Over the continental areas, the upper boundary is defined by topography and the lower boundary is the zero-elevation surface to which GTOPO30 is referenced. Over the oceanic areas the upper boundary is defined by the zero-elevation surface and the lower boundary by the bathymetry. The mass density of the topographic layer is set to the constant value of $\rho_{topo} = 2670$ kg/m^3 in the continental areas and for the oceanic areas the mass density of $\rho_{ocean} = -1750$

kg/m^3 is used. The goal of this test is not to represent the Earth's topography as accurately as possible, but to determine the effect of the number of binomial terms used for spectral forward modelling of the gravitational potential of such a layer. The gravitational field will be calculated on the geocentric sphere with the radius of $R = 6378.136$ km. This model fulfils the convergence criterion when a truncation limit of $\alpha = 3$ is used.

The first gravitational solution is constructed by using only the Stokes coefficients of the first binomial term. The second gravitational solution is constructed by including the Stokes coefficients of the first and second terms in the binomial series. This is repeated up to the truncation value $\alpha = 10$. The cut-off value of the spherical harmonic representation, l_{max}, is varied as 90, 180, 360, 720, 1200 and 1800, which corresponds to the approximated grid resolutions of 2, 1, 0.5, 0.25 and 0.1 arc-deg, respectively. The results are presented in Figure 4, which shows the maximum difference in the radial component of the gravitational acceleration vector. It can be seen that only the first two binomial series terms are needed to represent the gravitational field up to 180 degree and order accurately enough (± 1 mGal), as concluded by *Martinec et al.* (1989), *Rummel et al.* (1988), and *Balmino* (1994). More terms are needed when the resolution of the topographic model is increased. For example, a 0.1x0.1 arc-deg resolution model needs spherical harmonic coefficients up to degree and order 1800 to be represented correctly. This will result in 6 more binomial terms when an accuracy of ± 1 mGal is required, similar results were obtained by *Hirt and Kuhn* (2012).

4. Reducing the truncation error for deeper layers

To get insight into the numerical behaviour of the FSM for deeper mass layers that do not fulfil the convergence criterion, another modelling exercise is performed. The mass model consists of the same mass layer as in previous section, but now the zero-elevation reference is at 0, 50, 100, 200, 300 and 400 km depth. The computed gravitational fields should look similar, except for the damping effect of high degrees resulting from $\left(\frac{R}{r}\right)^{n+1}$ in Eq. (17). Figure 5a illustrates the degree variance of the spherical harmonic coefficients. At 0 km depth the degree variance follows approximately the Kaula rule as found by *e.g. Rummel et al.* (1988) and *Balmino et al.* (1973). The model at 50 km depth performs as expected with higher degree coefficients being damped more, as illustrated by an increasing difference between the blue and red line

for higher degrees. However, a different behaviour is seen for the layer at 100 km depth. From degree and order 100 onward, the degree variance stays flat. For deeper layers, the degree variance increases with degree, because the model does not fulfil the convergence criteria. This behaviour is also seen in the degree variances of the models at 200, 300 and 400 km depth, but with a different location of the 'bending' point. In the spatial domain these errors are seen to generate random-looking patterns with a slight correlation to the geometry of the modelled layer, as we will see in the benchmark (Section 5).

When fitting a forward gravity model to gravity field observations, these errors can lead to mismodelled densities. The errors arise because the density model does not fulfil the convergence criterion of Figure 3. In the following, we present a solution that reduces this error significantly and makes it possible to use the FSM forward modelling for global 3-D mass density models at any depth.

Because the error appears for deeper layers we introduce a new reference sphere R^*, such that the upper bound is reduced to approximately 0. Then, Eq. (6a) should be modified to

$$r_{upper} = R^* + U^*(\Omega') \tag{27a}$$

$$r_{lower} = R^* + L^*(\Omega') \ . \tag{27b}$$

The new spherical radius is defined as $R^* = R - \check{U}$, with $\check{U}$ being the maximum value of $U(\Omega')$. The new upper bound is defined with respect to the new spherical radius, $U^* = U - \check{U}$ and the new lower bound is defined as, $L^* = L - \check{U}$. From here, the method proceeds as before until Eq. (13). This relation now produces spherical harmonic coefficients with respect to the new reference sphere

$$\rho(\Omega')F^*(\Omega') \overset{GSHA}{=} \sum_{n,m}^{\infty} C^*_{nm} \ Y_{nm}(\Omega') \ . \tag{28}$$

Here F^* is defined based on the new U^*, L^*, and R^* values and C^*_{nm} are the coefficients referenced to the sphere with radius R^*. To transform these coefficients to the original reference sphere, R, the following relation is used:

$$C_{nm} = \left(\frac{R^*}{R}\right)^n \ C^*_{nm} \ . \tag{29}$$

These C_{nm} coefficients are now compatible with those in Eq. (13), or in other words, they are referenced to the original reference sphere with radius R.

To show the effect of the approach, we show the degree variance of the coefficients C_{nm} computed using the correction in Figure 5b. The expected damping of higher degree spherical harmonic coefficients is visible in contrast to Figure 5a. The method now seems to produce correct gravitational potential fields for density layers at any depth, because it fulfils the convergence criterion, as can be confirmed in Figure 3. To test this a benchmark is performed in the next section.

5. Benchmark

To benchmark the improved FSM forward modelling software, a comparison is performed to the tesseroid software used by *Kaban et al.* (2010). This software uses an algorithm which computes the combined gravitational effect of elementary volumes that make up a spherical Earth (*Artemjev and Kaban*, 1994). The algorithm is based on the equations of *Strakhov et al.* (1989), improved by *Kaban and Mooney* (2001) and *Kaban et al.* (2002). The benchmark will compare the vertical component of the gravitational accelerations, as computed from a density model on an equiangular 1x1 arc-deg grid, which corresponds to a maximum degree and order of 179 in spherical harmonics coefficients. The model takes the global Moho depth from CRUST1.0 global crustal model (*Laske et al.*, 2013) with the density contrast of 450 kg/m^3. The geometry is referenced to a sphere with a radius of 6371 km. Also, the gravitational field results are calculated on this reference sphere. To obtain an accuracy of <1 mGal, 8 binomial terms are included in the calculations for the spectral method, as deduced from inspection of Figure 4.

The benchmark is challenging, because of a difference in both forward modelling techniques. The tesseroid method uses a block representation, whereas the FSM approximates the geometry of the mass layer with spherical harmonic functions. To reduce this difference, we increased the resolution in the density models for the FSM solution. Figure 6 shows the difference between the geometries that are used by both methods for three spatial resolutions in the FSM, 1x1 arc-deg, 0.5x0.5 arc-deg, and 0.1x0.1 arc-deg. The higher resolution approximates the tesseroidal geometry much better. The high-resolution spectral geometry shows the well known Gibbs effects. However, the calculated gravity values are averaged over a 1x1 arc-deg potential field grid, therefore most of the Gibbs effect will be removed.

The results of the benchmark are shown in Figure 7. The 1x1 arc-deg potential field solution is compared to the tesseroid solution in Figure 7a

and d, without and with a correction, respectively. Figure 7d shows a slight improvement compared to the uncorrected result, which was expected after inspecting the convergence criterion, because models up to order and degree 180 in the spherical harmonics can have geometries up to 100 km deep, according to Figure 3. This particular Moho model stays well within the correct domain of the convergence criterion. Nevertheless, the maximum difference between the tesseroid and corrected spectral gravitational solutions is $\pm$ 60 mGal, which is around 10% of the signal. This difference can be attributed to the different approximation methods for the geometry (Figure 6) and is best visible in regions with large gradients in geometry.

This difference should be reduced after increasing the resolution of the spectral method. Figure 7b and e show the results using the 0.5x0.5 arc-deg grid without and with a correction, respectively. Here, the residuals of the comparison become smaller, which can be attributed to a better approximation of the shape of the Moho boundary. The proposed correction still does not have a great effect, because at many locations the convergence criterion is passed. Except at the Himalaya and the Andes Mountain Range some differences can be seen between the corrected and not-corrected solution.

The gravitational potential of an even higher resolution model compared to the tesseroid solution is shown in Figure 7c and f, without and with a correction, respectively. The effect of failing the convergence criterion is clear, differences of $\pm 10^6$ mGal are visible (Figure 7c). Thus, despite the increased spatial resolution, the fast spectral method performs much worse than the lower spatial resolution model. That is because, to represent the 0.1x0.1 arc-deg resolution, the spherical harmonics coefficients must be estimated up to 1800 degree. From the convergence criterion we learn that in that case the mass layer cannot deviate more than 10 km from the reference sphere (Figure 3). Yet, in the benchmark the Moho interface is on average 30 km deep, which causes this particular model to fail the convergence criterion and produce large errors.

After improving the forward modelling by lowering the reference sphere as explained in the previous section, the differences of the corrected solution with the benchmark stay between ± 2 mGal almost everywhere. We expect some higher variations for large gradients in the geometries such as in the Himalayas and the Andes (4 mGal). Furthermore, a large difference of 15 mGal is found at the North pole, which can be attributed to the high resolution of the tesseroid method there, because of the equiangular grid. The spectral method is unable to perfectly represent similar geometrical shapes, therefore

the gravitational effect at these locations is different. Moreover, Figure 7f shows a large correlation with the Moho geometry, which is also present in the 0.5x0.5 arc-deg solutions. This can be attributed to the Gibbs effect that is observed in Figure 6. These effects are not entirely symmetrical and will therefore not be averaged out completely. The resulting errors are below other gravity modelling errors. For example, *Mooney and Kaban* (2010) showed that errors due to uncertainty in sediment thickness will result in up to 12 mGal, uncertainty in Moho depth contributes to gravity anomalies of 30 mGal, and uncertainty in the thickness of the crystalline crust may reach up to 50 mGal.

Concluding, the benchmark shows that, despite the convergence error, the FSM can be improved to produce potential field solutions which differ from the tesseroid method less than the typical uncertainty in global gravity field modelling.

6. Conclusions

We have reviewed the fast forward gravitational modelling method using spherical harmonic representation (*Rummel et al.*, 1988). The FSM is capable of producing global gravitational potential fields from 3D-density structures after applying the correction proposed in this study. Because the results are computed in the form of spherical harmonic coefficients, they can be easily compared to geopotential models to which spectral filtering is applied. The method is computationally efficient compared to the rigorous spectral method in global topographic reductions.

Our analysis showed that the method is prone to large errors when modelling mass layers are situated at greater depths in the Earth, such as crustal and mantle layers. The error occurs due to truncation of the binomial series. A mitigation strategy for this depth-dependent error was devised by lowering the reference sphere during the global spherical harmonic analysis. This is followed by the transformation of the spherical harmonic coefficients back to the original sphere before their synthesis to a potential field. This strategy makes the spectral method capable of modelling the gravitational potential of mass density layers at any depth with the sufficient accuracy, as was demonstrated by benchmarking against a commonly used forward gravitational modelling software using tesseroids. The main difference between both methods is in the way how the geometry of the mass layers is approximated, where it can be argued that even though they imperfectly

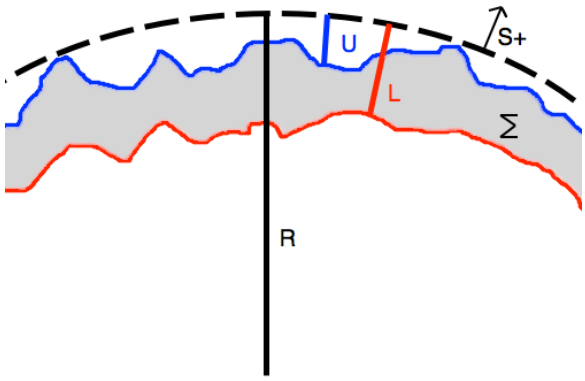

Figure 1: Sketch of of an arbitrary mass body. The distance (S) from the reference sphere R is defined positive upwards, resulting in $0 \geq U \geq L$.

represent tesseroids, spherical harmonics are not necessarily less suitable to represent density variations than tesseroids. Despite these differences, similar gravitational field solutions were constructed with a difference of only ± 4 mGal, which is well below other model errors. Thus the method can be used for constraining global density models of the crust and upper mantle with gravity data.

Acknowledgements

We would like to thank Roger Haagmans and Jörg Ebbing for discussion. Furthermore, we would like to thank the reviewer for the review of our manuscript. Funding was provided by NWO under the project ALW-GO-AO/10-10. P. Novák was supported by the project GA15-08045S of the Czech Science Foundation.

Appendix A. Introducing radial dependent mass density distribution

If the radial density distribution within a layer can be approximated by a polynomial model, then the following equations show how to use this particular distribution distribution with the FSM. The model was introduced for modelling atmospheric potential fields in *Novák* (2000). To simplify the derivation, a quadratic mass density distribution is taken:

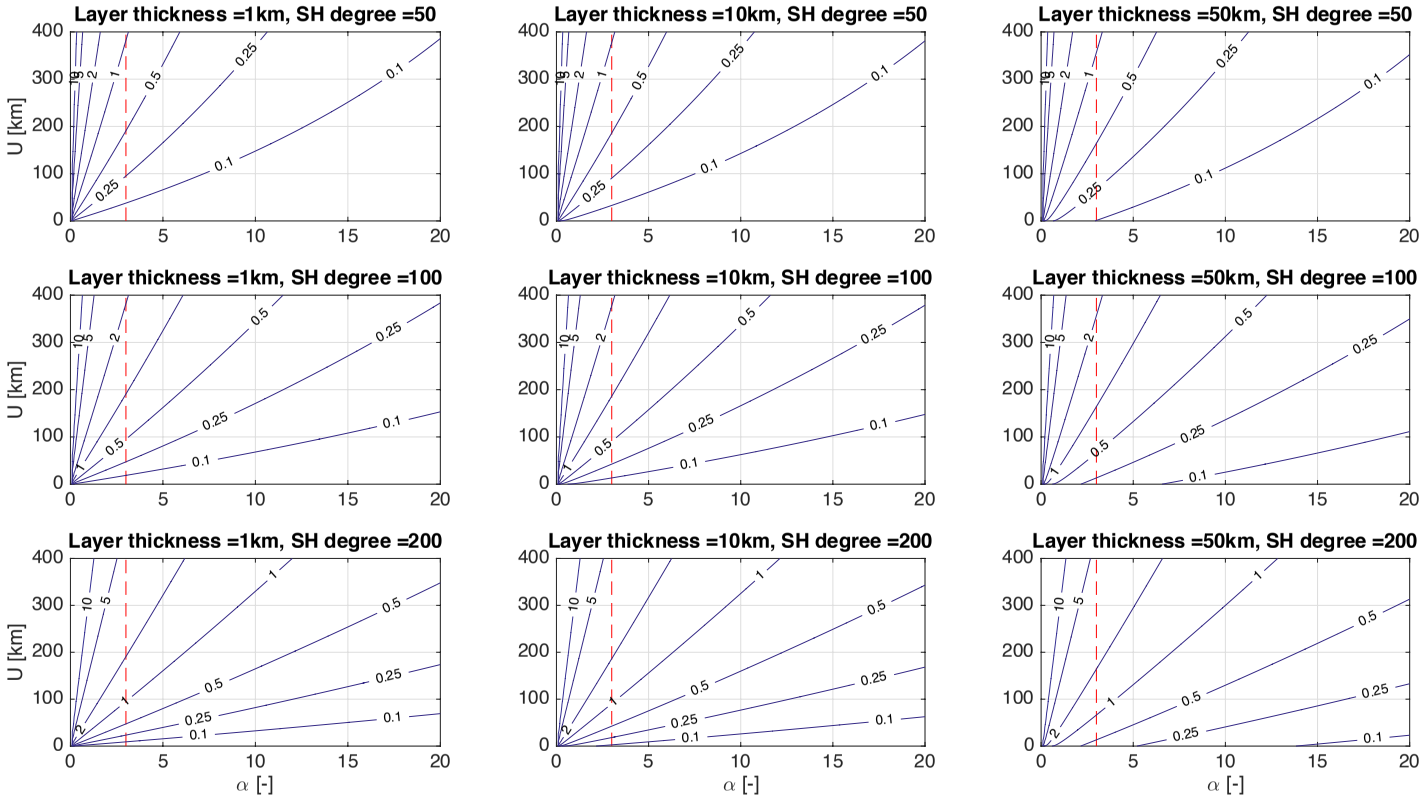

Figure 2: Contour plot of the values of $C^{(k)}$ as a function of U and α, for a number of values of the spherical harmonic degree $n = \nu - 3$ and layer thickness $|L - U|$. Dashed red lines indicate the currently typical $\alpha = 3$ truncation level.

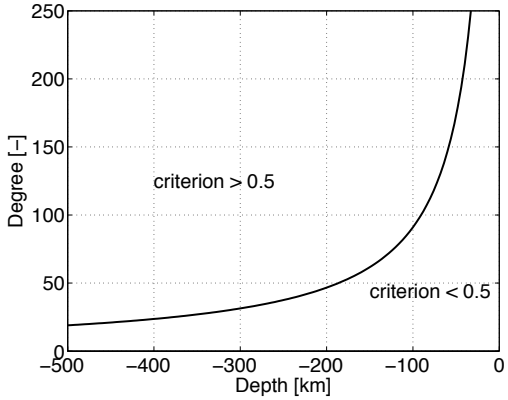

Figure 3: The boundary for an error criterion of $\frac{1}{2}$, as a function of the depth of the mass layer and the truncation limit. The depth represents the value of U and a truncation limit of $\alpha = 3$ is chosen.

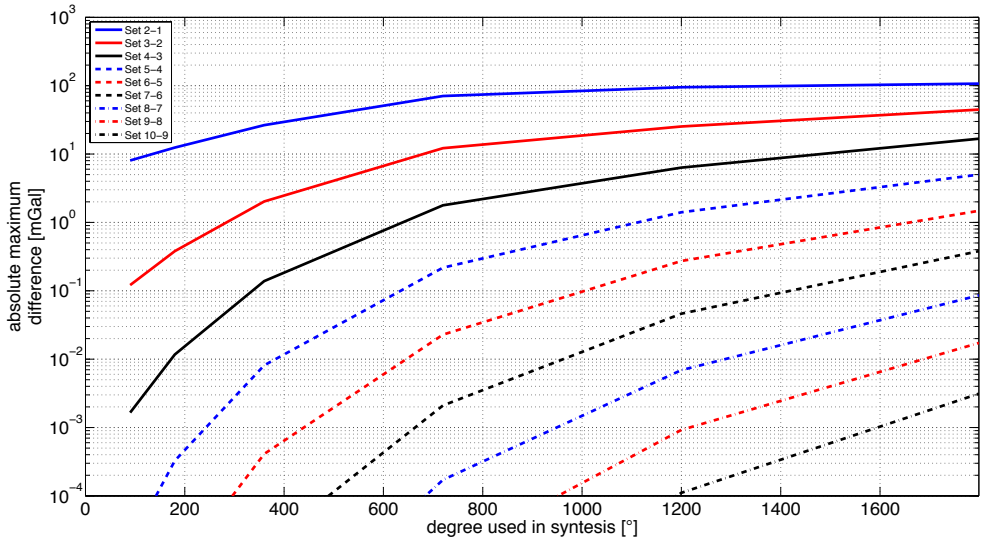

Figure 4: Difference between two gravitational solutions using a different number of binomial series term approximations as depicted in the legend.

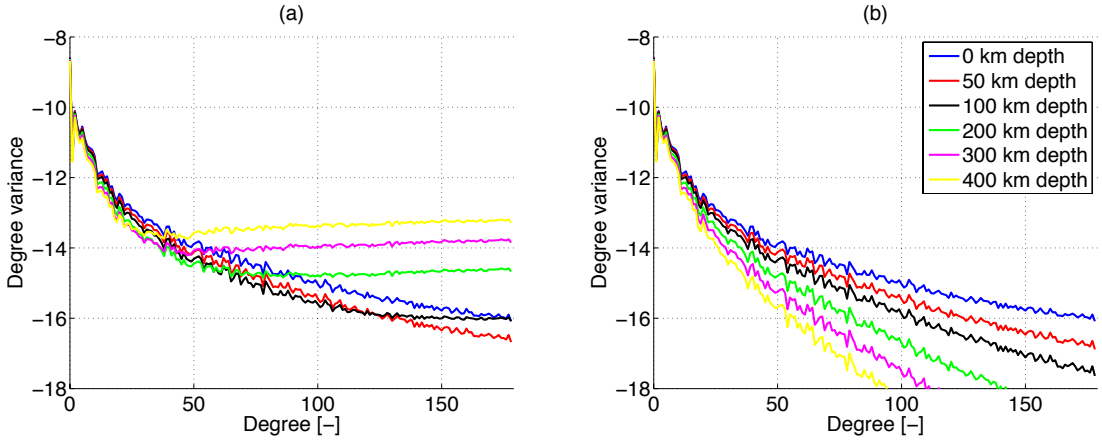

Figure 5: The degree variance of the spherical harmonic coefficients of the gravitational potential derived from the topographic mass density layer for different depths: 0, 50, 100, 200, 300 and 400 km: (a) without correction, and (b) with correction.

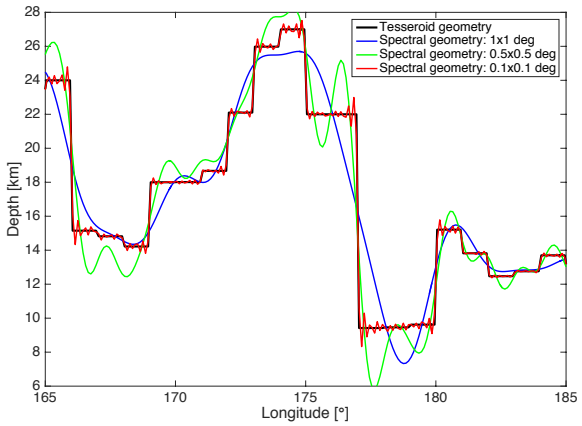

Figure 6: A cross section of the different Moho geometries used in the benchmark. The black line represents the tesseroid geometry approximation, the blue line represents the spherical harmonic geometry approximation with the 1x1 arc-deg resolution, the green line represents the spherical harmonic geometry approximation with the 0.5x0.5 arc-deg resolution, and the red line represents the spherical harmonic geometry approximation with the 0.1x0.1 arc-deg resolution.

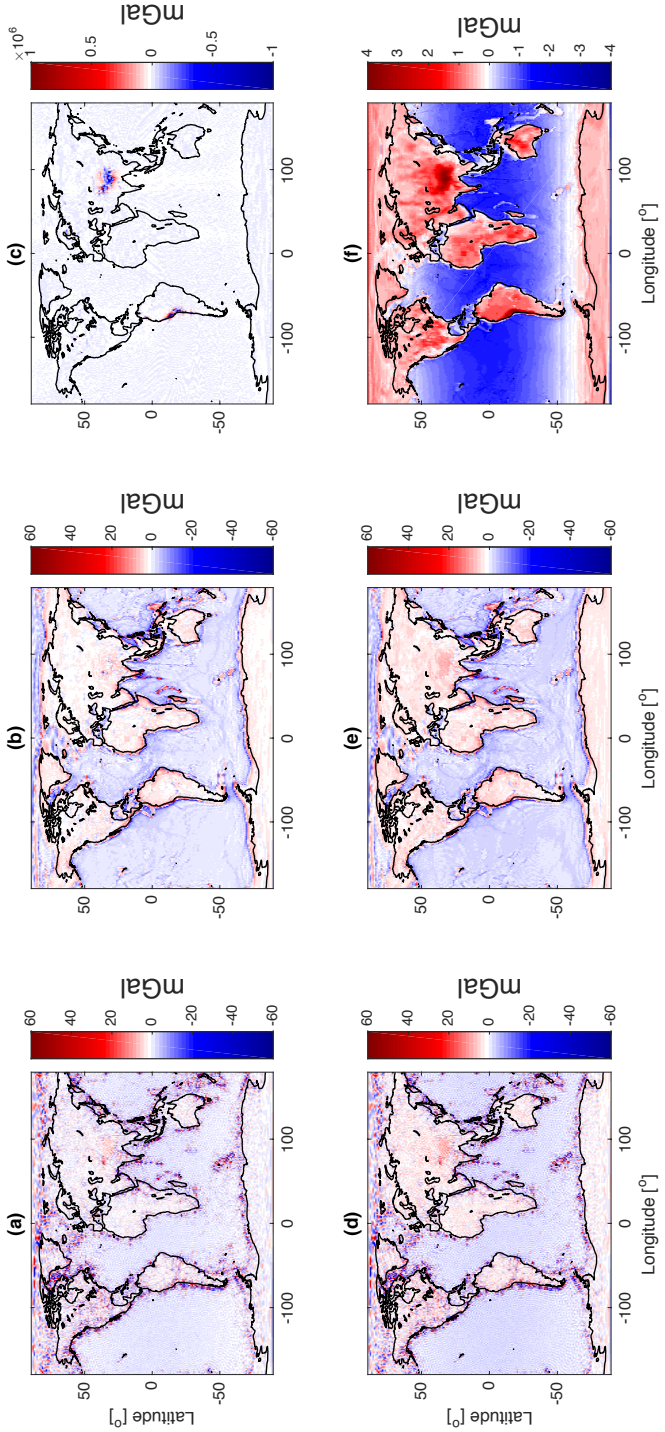

Figure 7: The difference between the tesseroid and the FSM forward modelling technique for (a) a 1x1 arc-deg spatial resolution without correction, (b) a spatial resolution of 0.5x0.5 arc-deg without correction, (c) a spatial resolution of 0.5x0.5 arc-deg without correction, and (d) a spatial resolution of 1x1 arc-deg with correction, (e) a spatial resolution of 0.5x0.5 arc-deg with correction, (f) a spatial resolution of 0.1x0.1 arc-deg with correction.

$$\rho(r',\Omega') = \rho_0(\Omega')\ [\ 1 + a\ (R - r') + b\ (R - r')^2\ ] \tag{A.1}$$

where $\rho_0(\Omega')$ is the mass density of the layer at $r' = R$, i.e. at the reference sphere and α and β are defined as:

$$a = \frac{\mathrm{d}\rho}{\mathrm{d}r'}\ \frac{1}{\rho_0}\ , \tag{A.2a}$$

$$b = \frac{\mathrm{d}^2\rho}{\mathrm{d}r'^2}\ \frac{1}{\rho_0}\ . \tag{A.2b}$$

When the mass density is dependent on r', the derivation of the FSM deviates starting from the radial integral in Eq. (5), because the mass density is now inside the integral:

$$\int_{r_{lower}(\Omega')}^{r_{upper}(\Omega')} \rho(r',\Omega')\ r'^{n+2}\mathrm{d}r'\ . \tag{A.3}$$

Substituting Eq. (A.1) in the multiplication inside the integral as follows

$$\rho(r',\Omega')\ r'^{n+2} = \rho_0(\Omega')\ [\ r'^{n+2} + (a\ R + b\ R^2)\ r'^{n+2} - (a + 2b\ R)\ r'^{n+3} + b\ r'^{n+4}]\ . \tag{A.4}$$

Then, (A.3) becomes

$$\begin{aligned}\rho_0(\Omega')\Big\{ &\frac{1 + aR + bR^2}{n+3} && \Big[(R + U(\Omega'))^{n+3} - (R + L(\Omega'))^{n+3}\Big] \\ &- \frac{a + 2bR}{n+4} && \Big[(R + U(\Omega'))^{n+4} - (R + L(\Omega'))^{n+4}\Big] \\ &+ \frac{b}{n+5} && \Big[(R + U(\Omega'))^{n+5} - (R + L(\Omega'))^{n+5}\Big]\Big\}\end{aligned} \tag{A.5}$$

The relation can be simplified by the same procedure as previously using the binomial series expansion. After truncating the binomial series the radial integral eventually results in

$$\begin{aligned}\rho_0(\Omega')\ R^{n+3}\Big\{ &\frac{(U - L)}{R} + \frac{(n+2) - aR}{2R^2}(U^2 - L^2) \\ &+ \frac{(n+2)(n+1) - 2(n+2)aR + 2bR^2}{6R^3}(U^3 - L^3)\Big\}\ .\end{aligned} \tag{A.6}$$

Equation A.6 is similar to Eq. (10) but with extra terms resulting from the polynomial density gradient coefficients. After this, the derivation proceeds as for the FSM for layers with constant density. The second-order polynomial coefficients, a and b, are visible in the second and third terms of the binomial series expansion. When examining this further, higher-order polynomial coefficients would modify the fourth and higher terms of the binomial expansion. When only three terms are used in the series expansion, a cubic polynomial for the radial mass density distribution cannot be used.

References

Abramowitz, M. and Stegun, I., editors (1972). *Handbook of Mathematical Functions: with Formulas, Graphs, and Mathematical Tables*. New York: Dover.

Artemjev, M.E. and Kaban, M.K. (1994). Density inhomogeneities, isostasy and flexural rigidity of the lithosphere in the Transcaspian region. *Tectonophysics*, 240, 281–297.

Balmino, G., Lambeck, K., and Kaula, W. M. (1973). A spherical harmonic analysis of the Earth's topography. *Journal of Geophysical Research*, 78(2), 478–481.

Balmino, G. (1994). Gravitational potential harmonics from the shape of a homogeneous body. *Celestial Mechanics and Dynamical Astronomy*, 60, 331–364.

Claessens, S.J. and C. Hirt (2013). Ellipsoidal topographic potential: New solutions for spectral forward gravity modeling of topography with respect to a reference ellipsoid, *Journal of Geophysical Research*, 118, 5991-6002.

Heiskanen, W.A. and Moritz, H. (1984). *Physical Geodesy*, Reprint, Institute of Physical Geodesy, Technical University Graz, Austria.

Hirt, C. and M. Kuhn (2012). Evaluation of high-degree series expansions of the topographic potential to higher-order powers *Journal of Geophysical Research*, 117, B12407.

Kaban, M.K. and Mooney, W. (2001). Density structure of the lithosphere in the southwestern United States and its tectonic significance *Journal of Geophysical Research*, 106, 721–740.

Kaban, M.K., Flovenz, O.G., and Palmason, G. (2002). Nature of the crust-mantle transition zone and the thermal state of the upper mantle beneath Iceland from gravity modelling. *Geophysical Journal International*, 149, 281–299.

Kaban, M.K., Tesauro, M., and Cloetingh, S. (2010). An integrated gravity model for Europe's crust and upper mantle. *Earth and Planetary Science Letters*, 296, 195–206.

Lachapelle, G. (1976). A Spherical Harmonic Expansion of the Isostatic Reduction Potential. *Bollettino di Geodesia E Scienze Affini*, nr. 3.

Laske, G., Masters, G., Ma, Z. and Pasyanos, M. (2013). Update on CRUST1.0 - A 1-degree Global Model of Earth's Crust. *Geophys. Res. Abstracts*, (15), Abstract submitted to EGU2013-2658.

Martinec, Z., Pec, K., and Bursa, M. (1989). The Phobos gravitational field modeled on the basis of its topography. *Earth, Moon, and Planets*, 45, 219–235.

Martinec, Z. (1991). On the accuracy of the method of condensation of the Earth's topography. *Manuscripta Geodaetica*, 16, 288–294.

Mooney, W. and M.K. Kaban (2010). The North American Upper Mantle: Density, Composition, and Evolution, *Journal of Geophysical Research*, 115, B12424.

Novák, P (2000). Evaluation of gravity data for the Stokes-Helmert solution to the geodetic boundary-value problem. *Technical Report 207*, University of New Brunswick, Fredericton.

Novák, P. and Grafarend, E. (2006). The effect of topographical and atmospheric masses on space borne gravimetric and gradiometric data. *Studia Geophysica et Geodaetica*, 50, 549–582.

Pavlis, N.K. and Rapp, R.H. (1990). The development of an isostatic gravitational model to degree 360 and its use in global gravity modelling. *Geophysical Journal International*, 100, 369–378.

Rapp, R. H. (1982). Degree variances of the Earth's potential, topography and its isostatic compensation. *Bulletin Géodésique*, 56, 84–94.

Root, B. C., Ebbing, J., van der Wal, W., Novák, P., and Vermeersen, L. (2015). Glacial isostatic adjustment in the static gravity field of Fennoscandia. *Journal of Geophysical Research: Solid Earth*, 120, 503-518.

Rummel, R., Rapp, R. H., Sunkel, H., and Tscherning, C. C. (1988). Comparison of global topographic/isostatic models to the Earth's observed gravity field. *Technical Report Report No. 388*, Department of Geodetic Science and Surveying, The Ohio State University Columbus, Ohio.

Sneeuw, N. (1994). Global spherical harmonic analysis by least-squares and numerical quadrature methods in historical perspective. *Geophysical Journal International*, 118, 707–716.

Strakhov, V.N., Romaniuk, T.V., and Frolova, N.K. (1989). Method of direct gravity problem solution for modeling of global and regional gravity anomalies (in Russian) In: Strakhov, V. (Ed.) *New Methods of the Gravity and Magnetic Anomaly Interpretation*, Inst. Whys. of the Earth, Moscow, pp. 118–235.

Vaníček, P., Najafi, M., Martinec, Z., Harrie, L., and Sjöberg, L. E. (1995). Higher-degree reference field in the generalized Stokes-Helmert scheme for geoid computation. *Journal of Geodesy*, 70(1), 176–182.